

# Subspace decomposition with defect diffusion coefficient

Dilini Kolombage<sup>‡</sup>

Axel Målqvist<sup>†</sup>

Barbara Verfürth<sup>‡</sup>

**Abstract.** Elliptic diffusion problems with multiscale heterogeneous coefficients lead to poorly conditioned discrete systems and therefore require effective preconditioning strategies. While subspace decomposition preconditioners perform well for fixed realizations of the coefficient, their repeated construction becomes prohibitively expensive in uncertainty quantification settings, particularly in Monte-Carlo simulations, where a large number of fine-scale realizations must be treated. In this paper, we propose an offline-online approximation of a subspace decomposition preconditioner that exploits the localized structure of the random defects. The preconditioner is constructed from local subspace solves that are precomputed offline for a small set of reference configurations and efficiently combined online for arbitrary realizations. We analyze the spectral properties of the resulting offline-online approximation operator and confirm its robustness and efficiency through numerical experiments.

**Key words.** preconditioner; subspace decomposition; perturbed problem; offline-online strategy; domain decomposition

**AMS subject classifications.** 65N55, 65N30, 65N12, 35J15, 35B20, 35R60

## 1 Introduction

Elliptic diffusion problems with heterogeneous coefficients arise in a wide range of applications including composite materials, porous structures and many environmental models. Due to the strong heterogeneity and possible high contrast of these coefficients, often characterized by multiple scales, such problems typically lead to large ill-conditioned linear systems, for which iterative solvers require suitable preconditioning to achieve robust convergence. Domain decomposition and subspace correction methods are standard tools in this regard, as they provide effective preconditioners based on coarse corrections and localized subdomain solves, see [22, 18].

For a single realization of the coefficient, these approaches are well understood and can be applied effectively in combination with standard finite element discretizations. However, when many realizations of the defect configuration must be treated — for instance in Monte-Carlo (MC) sample simulations — the repeated construction of high quality, realization-dependent preconditioners becomes prohibitively expensive since the setup of domain decomposition methods involves many fine scale local factorizations or inversions. This motivates amortized strategies, in which expensive local computations are performed offline and then reused across many solves.

Existing work addresses this challenge through different reuse mechanisms. Closest in spirit to the present work are methods that combine domain decomposition with an offline-online split. In these approaches, key local domain decomposition ingredients, such as Schur complements or influence operators, are approximated offline by low-dimensional surrogate models, and then these surrogates are evaluated cheaply for each realization during sampling. In [19, 3], a polynomial chaos (PC) expansion computation is done on non-overlapping subdomains in a pre-processing stage that will be used in the MC sampling stage. Related ideas have also been proposed in [23] in the context of stochastic balancing domain decomposition by constraints (BDDC) methods, where local polynomial chaos surrogates are built offline using Karhunen–Loève (KL) parametrization which are then used online to efficiently assemble the sample-dependent BDDC preconditioner at low cost for each realization.

Further approaches have been proposed that are conceptually different from the present work, yet address the same challenges. In [25], the authors introduce a finite library of offline preconditioners by clustering (quantizing) the random coefficients via a truncated KL representation and Voronoi cells, and use the nearest centroid coefficient to choose which preconditioner to apply. Nearby preconditioning

---

<sup>‡</sup>Institute for Numerical Simulation, University of Bonn, Friedrich-Hirzebruch-Allee 7, 53115 Bonn, Germany.

<sup>†</sup>Department of mathematical sciences, Chalmers University of Technology and University of Gothenburg, Chalmers Tvärgata 3, 41296 Göteborg, Sweden.

methods introduced in [15] solve the stochastic Helmholtz equation and reuse a preconditioner constructed for one realization to accelerate the solve for another realization whenever the coefficients are sufficiently close in an appropriate norm. A different line of work studied in [4, 16] treats randomness by stochastic Galerkin or spectral discretizations in the stochastic variable, leading to one large coupled deterministic system and motivating mean-based block preconditioners with detailed eigenvalue analysis. In an alternative formulation introduced in [9, 10], the stochastic elliptic PDE is rewritten as a sequence of deterministic systems (KL and a double-orthogonal polynomial basis) and accelerates their solution with additive Schwarz combined with Krylov-subspace recycling. A wide range of further preconditioning techniques for stochastic Galerkin systems are studied in [2, 17, 24, 21, 20].

This present study is largely motivated by composite materials with a periodic (or engineered) microstructure in which manufacturing damage or impurities introduce rare localized defects. In such media, most cells coincide with a fixed background configuration, while only a small subset contains erasures at weakly randomized locations. Figure 1.1 illustrates a typical realization of such a random erasure model in two dimensions. Compared to the aforementioned approaches, the present work, therefore, exploits a qualitatively different source of structure. Existing offline-online domain decomposition and stochastic BDDC methods build surrogate models for interface or Schur complement operators in a parametrized random-field setting, and their cost and complexity typically scale with the dimension of this global stochastic parametrization. On the other hand, other existing approaches rely on quantitative notions of closeness between realizations, which are not directly applicable in settings with localized coefficient variations, where realizations are not naturally ordered by a global proximity measure. Here we instead consider diffusion coefficients with a periodic background perturbed by localized random defects, occurring with a fixed probability  $p$ . Similar to the weakly random setting of [1], the diffusion coefficient is given by

$$A(x, \omega) = A_\varepsilon(x) + b_{p,\varepsilon}(x, \omega) B_\varepsilon(x) \tag{1.1}$$

where  $A_\varepsilon$  represents a periodic background coefficient,  $B_\varepsilon$  describes the localized defect contribution, and  $b_{p,\varepsilon}$  is a random indicator function encoding the presence or absence of defects on the periodic cells with a given probability  $p$ . We leave the rigorous definitions to Section 2. The resulting randomness is therefore highly localized and combinatorial in nature, rather than being described by a global random field with long-range correlations. Importantly, while the fine mesh resolves the localized inclusions, the coarse mesh does not, and interior coarse-scale patches differ only through the local defect configurations they contain. In this regime, the number of distinct local configurations is small and does not grow with the number of samples, which allows us to construct patch-local preconditioner blocks once for a finite dictionary of defect patterns and then reuse them algebraically to construct all patches and realizations at a minimal cost. This directly supports an efficient approximation of the additive Schwarz preconditioners for elliptic problems, since their local patch solves depend only on the coefficient restricted to each patch.

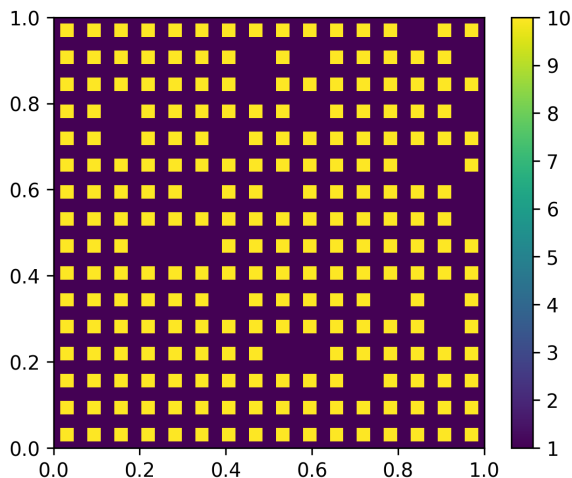


Figure 1.1: The random erasure model in two-dimension with  $\alpha = 1$ ,  $\beta = 10$ ,  $p = 0.1$ ,  $\varepsilon = 2^{-4}$  and  $h = 2^{-9}$ .

Building on this observation, we propose an additive Schwarz type offline-online overlapping domain decomposition preconditioner tailored to defect-type randomness. Unlike the surrogate based methods, which approximate operators for global random parameter, our method relies only on a small set of local reference defects induced by the periodic background. In the offline stage we compute and store patch local factorizations for these single-defect reference coefficients including the defect free background. In the online stage, for each realization and each patch, the local preconditioner contributions are assembled purely algebraically as combinations and permutations of these precomputed operators, without additional patch local solves. The coarse component is treated analogously through an element-wise offline-online assembly but exactly.

The key contribution of this work is to incorporate local defects into a rigorous and efficient approximation of the two-level additive Schwarz preconditioner. We show that the proposed offline-online construction yields an operator  $\tilde{\mathcal{B}}(A)$  that can be interpreted as a perturbation of the additive Schwarz preconditioner  $\mathcal{B}(A)$ , and we derive bounds relating the spectral behaviour of  $\tilde{\mathcal{B}}(A)$  and the convergence of the preconditioned conjugate gradient (PCG) method to the offline-online approximation error. Numerically, we demonstrate that  $\tilde{\mathcal{B}}(A)$  performs close to  $\mathcal{B}(A)$  across varying defect probabilities and contrasts, while substantially reducing setup cost compared to the exact preconditioner, and outperforming the reuse of a single defect-free preconditioner. To assess the performance of our preconditioner across different complexity levels, we additionally test it on several defect geometries.

The remainder of this paper is organized as follows. In Section 2, we introduce the model problem and the subspace decomposition framework that forms the basis of our offline-online method considered in this work. Section 3 presents the proposed offline-online strategy for approximating the exact subspace decomposition preconditioner in detail. In Section 4, we analyse the spectral properties of the preconditioned operator and the convergence results of the preconditioned conjugate gradient method. Implementation aspects and a detailed run-time complexity analysis are discussed in Section 5. Numerical experiments illustrating the performance of the offline-online method in comparison to several base methods are presented in Section 6. Finally, Section 7 concludes the paper with a summary and outlook.

## 2 Subspace decomposition framework

In this section, we introduce the model problem, its finite element discretization, and the subspace decomposition framework – following [13, 5] – that form the basis of the method proposed in this paper. The purpose of this section is to fix notation and recall standard concepts.

### 2.1 Model problem

Let  $\Omega \subset \mathbb{R}^d$ ,  $d \in \{1, 2, 3\}$ , be a bounded Lipschitz domain. We define

$$H^1(\Omega) := \{v \in L^2(\Omega) : \nabla v \in [L^2(\Omega)]^d\},$$

where  $V := H_0^1(\Omega)$  denotes the subspace of  $H^1(\Omega)$  consisting of functions with vanishing trace on  $\partial\Omega$ . We consider the diffusion problem: find  $u \in V := H_0^1(\Omega)$  such that

$$a(u, v) := \int_{\Omega} A \nabla u \cdot \nabla v \, dx = \int_{\Omega} f v \, dx =: (f, v) \quad \forall v \in V, \quad (2.1)$$

where  $f \in L^2(\Omega)$  and the diffusion coefficient  $A \in L^\infty(\Omega)$  satisfies the uniform ellipticity bounds  $0 < \alpha \leq A(x) \leq \beta$  for almost every  $x \in \Omega$ . The associated energy norm is given by  $\|v\|_a := a(v, v)^{1/2}$ . In this paper, we consider a random diffusion coefficient  $A(x, \omega)$ , where the above properties hold uniformly in the random variable  $\omega$ . The precise model, also considered in [14, 12], is given by

$$A(x, \omega) = A_\varepsilon(x) + \sum_{i \in I \subset \mathbb{Z}^d} \chi_{\varepsilon(i+Q)}(x) \hat{b}_p^i(\omega) B_\varepsilon(x). \quad (2.2)$$

Here,  $A_\varepsilon$  and  $B_\varepsilon$  are  $\varepsilon$ -periodic functions,  $Q \subseteq [0, 1]^d$  denotes a reference cell, and  $\{\hat{b}_p^i\}_{i \in I}$  are independent Bernoulli random variables with probability  $p$ . The coefficient  $A_\varepsilon$  represents a periodic background medium, while the second term introduces localized defect inclusions of identical shape and size, randomly activated with probability  $p$ . This setup is illustrated in Figure 1.1.

We discretize  $\Omega$  using a fine Cartesian mesh  $\mathcal{T}_h$  that resolves all microscale features of the coefficient  $A$  and define the conforming finite element space  $V_h \subset V$  consisting of continuous, piece-wise bilinear functions, i.e.,  $Q1$  elements on the mesh. The corresponding discrete problem reads: find  $u_h \in V_h$  such that

$$a(u_h, v) = (f, v) \quad \forall v \in V_h. \quad (2.3)$$

In addition, we introduce a nested coarse mesh  $\mathcal{T}_H$  with mesh size  $H > h$ , and denote by  $V_H \subset V_h$  the associated coarse finite element space. Throughout the paper, we assume that  $\mathcal{T}_h$  is a refinement of  $\mathcal{T}_H$ .

## 2.2 Patch structure and subspaces

In this section we introduce the patch geometry required to define the subspaces. The construction is valid for dimensions  $d \leq 3$ , where the computational domain  $\Omega \subset \mathbb{R}^d$  is assumed to be a (unit) hypercube equipped with the uniform cartesian meshes  $\mathcal{T}_H$  and  $\mathcal{T}_h$ . For the clarity of demonstration, all illustrations in this paper are depicted in two dimensions.

In the subspace decomposition framework, the fine-scale space is decomposed into overlapping local subspaces associated with subdomains  $\omega_i \subset \Omega$  defined around the vertices of the coarse mesh. Let  $\{\varphi_i\}_{i \in \mathcal{N}}$  denote the nodal basis of the coarse space  $V_H$ , where  $\mathcal{N}$  is the index set of coarse interior vertices. For each  $i \in \mathcal{N}$ , we define the corresponding subdomain, (hereafter also referred to as a patch)

$$\omega_i := \text{supp}(\varphi_i),$$

that is, the union of all coarse elements sharing the vertex associated with  $\varphi_i$ . Using these patches, we define a family of local subspaces

$$V_i := V_h \cap H_0^1(\omega_i), \quad i \in \mathcal{N},$$

and set  $V_0 := V_H$ . The collection  $\{V_i\}_{i=1}^{|\mathcal{N}|}$  forms an overlapping decomposition of the fine-scale space  $V_h$ . The patches  $\omega_i$  are assumed to have uniformly bounded overlap, that is, each point in  $\Omega$  is contained in at most a fixed number of patches independent of  $h$  and  $H$ . For illustration, Figure 2.1 shows the construction of vertex-centered patches on a uniform coarse mesh. Consequently, the patches share identical structure up to translation, which will be exploited in Section 3 to construct approximate local operators via an offline-online strategy.

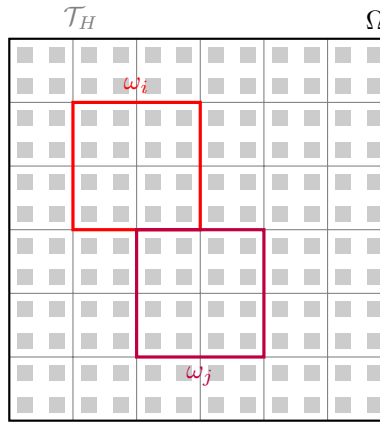


Figure 2.1: Possible pattern of a coefficient  $A_\varepsilon$  and the patches  $\omega_i$ .

**Remark 2.1.** Although our current study assumes hypercube domains equipped with uniform cartesian meshes for simplicity, the underlying subspace decomposition framework can be extended to more general Lipschitz domains. In such cases, the patches as defined above, may no longer be identical up to translation (depending on the mesh structure). Consequently, the translation-invariant property exploited in the offline-online strategy may be weakened. However, this can be addressed by introducing a few additional reference configurations or treating the affected patches separately, still retaining the overall efficiency of the offline-online approach if the domain is not too complicated.

### 2.3 Local projections and additive preconditioner

From this point on, all operators and spaces are understood on the discrete finite element spaces  $V_h$  and  $V_H$ , as required. Recall that  $(\cdot, \cdot)$  denotes the  $L^2(\Omega)$  inner product. We let  $V'_h$  be the dual space of  $V_h$  and introduce by  $\langle \cdot, \cdot \rangle : V'_h \times V_h \rightarrow \mathbb{R}$  the associated duality pairing. We can then identify  $f \in L^2(\Omega)$  with an element of  $V'_h$  via

$$\langle f, v \rangle := (f, v) \quad \forall v \in V_h.$$

We further introduce the linear operator  $\mathcal{L} : V_h \rightarrow V'_h$  associated with the bilinear form  $a(\cdot, \cdot)$

$$\langle \mathcal{L}v, w \rangle := a(v, w) \quad \forall v, w \in V_h.$$

Next, for each subspace  $V_i$  for  $i = 1, \dots, |\mathcal{N}|$ , we define the local solution operator  $\mathcal{B}_i : V'_h \rightarrow V_i$  by

$$a(\mathcal{B}_i g, w) = \langle g, w \rangle \quad \forall w \in V_i \quad (2.4)$$

for given  $g \in V'_h$ . Our aim is to apply  $\mathcal{B}_i$  to the functional of the form  $g = \mathcal{L}v$  yielding the associated local Ritz projection  $\mathcal{P}_i : V_h \rightarrow V_i$  defined by

$$\mathcal{P}_i = \mathcal{B}_i \circ \mathcal{L},$$

and is equivalent to the variational characterization

$$a(\mathcal{P}_i v, w) = a(v, w) \quad \forall w \in V_i. \quad (2.5)$$

Then the associated additive subspace decomposition operator is given by

$$\mathcal{P} := \sum_{i=0}^{|\mathcal{N}|} \mathcal{P}_i = \mathcal{B} \circ \mathcal{L}, \quad \text{with} \quad \mathcal{B} := \sum_{i=0}^{|\mathcal{N}|} \mathcal{B}_i$$

where the index  $i = 0$  corresponds to the coarse space  $V_0 := V_H$ . The associated operator  $\mathcal{B}_0 : V'_h \rightarrow V_H$  is defined analogously to the local operators  $\mathcal{B}_i$  by solving a variational problem on the coarse space. It represents the global, coarse-scale correction in the subspace decomposition, while the operators  $\mathcal{B}_i$ ,  $i \geq 1$ , provide localized fine-scale corrections supported on the patches  $\omega_i$ .

On the discrete level, the variational problem is solved by a preconditioned conjugate gradient method using  $\mathcal{B}$  as a left preconditioner. The operator  $\mathcal{P} = \mathcal{B} \circ \mathcal{L}$  is not formed explicitly and is introduced only for analytical purposes: it represents the preconditioned operator associated with the bilinear form  $a(\cdot, \cdot)$ . Classical convergence results for PCG can be expressed in terms of spectral properties of  $\mathcal{P}$ , and this viewpoint will be used in the convergence analysis in Section 4. In the ideal case, the operators  $\mathcal{B}_i$  and  $\mathcal{B}_0$  are computed with respect to the true coefficient  $A$ , leading to a preconditioner with favorable robustness and scalability properties. However, in the presence of random defects, the direct construction of all local operators becomes computationally expensive.

## 3 Offline-online approximation of the preconditioner

In this section, we address the efficient construction of the subspace preconditioner in the presence of random defect coefficients. Building on the exact framework introduced in Section 2, our goal is to approximate the local operators  $\mathcal{B}_i$  and assemble a computationally efficient preconditioner without sacrificing the properties of the original method. More precisely, we retain the exact coarse operator  $\mathcal{B}_0$ , while the patch-local operators  $\mathcal{B}_i$ ,  $i \geq 1$ , are approximated by an offline-online strategy that exploits the localized structure of the defect coefficient. To highlight that the operators  $\mathcal{B}_i$  depend on the (realization of the) diffusion coefficient  $A$ , we will sometimes write  $\mathcal{B}_i(A)$  in the following.

We assume that the coarse mesh  $\mathcal{T}_H$  is aligned with the periodicity of  $A_\varepsilon$  in the sense that the restriction  $A_\varepsilon|_K$  is identical for all coarse elements  $K \in \mathcal{T}_H$ . Furthermore, we assume a scale separation of the form

$$h \leq \varepsilon < H,$$

where  $\varepsilon$  is not asymptotically small with respect to  $H$ . This regime is typical for defect problems, in which the microscale is resolved on the fine mesh but does not average out on the coarse scale.

We further recall from Section 2.2 that all patches share the same geometry up to translation. The localized and repetitive structure of the defect term is the key property that enables an efficient offline-online strategy. Rather than constructing all local operators  $\mathcal{B}_i$  from scratch for each realization of the coefficient, we exploit the fact that local problems on interior patches depend only on the restriction of  $A$  to those patches. This observation forms the basis of the offline-online approximation described in the remainder of this section.

### 3.1 Offline phase

In the offline phase we compute a set of local operators corresponding to a finite collection of reference coefficients. These operators are reused in the online phase to construct approximations of patch-local operators for arbitrary defect realizations.

Due to the periodic structure of the background coefficient  $A_\varepsilon$  and the identical shape and size of the defect inclusions, all interior patches  $\omega_i$  share the same geometric structure up to translation, as illustrated in Figure 2.1. Moreover, for any interior patch, the restriction of the coefficient  $A(\cdot, \omega)$  to  $\omega_i$  is fully determined by the local defect configuration within the patch. This allows local problems posed on different interior patches to be mapped, by translation, to a single reference patch. Moreover, the defect term in (2.2) has a localized structure. Therefore, the restriction of the coefficient to an interior patch  $\omega_i$  can be represented as a sum of contributions corresponding to individual defect locations.

In the offline phase, we therefore introduce a finite family of reference coefficients defined on a reference patch  $\widehat{\omega}$ . The first reference coefficient corresponds to the defect-free background,

$$A^{(0)} := A_\varepsilon|_{\widehat{\omega}}.$$

For each admissible defect location intersecting the patch, we define its reference coefficient

$$A^{(\ell)} := A_\varepsilon|_{\widehat{\omega}} + \chi_{\varepsilon(j_\ell+Q)} B_\varepsilon, \quad \ell = 1, \dots, \mathbf{N}_{\text{ref}},$$

where  $j_\ell$  enumerates the possible defect positions within  $\widehat{\omega}$ . In this way, the set  $\{A^{(\ell)}\}_{\ell=0}^{\mathbf{N}_{\text{ref}}}$  exhaustively covers all possible defect locations on the patch via single-defect configurations. No multi-defect coefficients are stored in the offline phase.

Now, we can define the corresponding reference local solution operators for these reference coefficients  $A^{(\ell)}$ ,  $\ell = 0, \dots, \mathbf{N}_{\text{ref}}$ , by solving a local variational problem on the reference patch  $\widehat{\omega}$ .

Let  $\widehat{V} \subset H_0^1(\widehat{\omega})$  denote the finite element space on the reference patch. For a given functional  $g \in \widehat{V}'$ , the reference local solution operator

$$\widehat{\mathcal{B}}^{(\ell)} : \widehat{V}' \rightarrow \widehat{V}$$

is defined by

$$\int_{\widehat{\omega}} A^{(\ell)} \nabla(\widehat{\mathcal{B}}^{(\ell)} g) \cdot \nabla w \, dx = \langle g, w \rangle \quad \forall w \in \widehat{V}. \quad (3.1)$$

The operators  $\widehat{\mathcal{B}}^{(\ell)}$  correspond to the exact local factorizations associated with the defect-free background ( $\ell = 0$ ) and with exactly one defect located at each admissible defect-location within the reference patch ( $\ell \geq 1$ ). They are computed once in the offline phase and stored for later use.

### 3.2 Online phase

Given a realization of the coefficient  $A(\cdot, \omega)$ , the restriction of  $A$  to an interior patch  $\omega_i$  can be represented in terms of the reference coefficients introduced in the offline phase. Each defect intersecting the patch activates exactly one single-defect reference coefficient, while the remaining contribution is accounted for by the defect-free background coefficient. In mathematical terms, this can be written as

$$A|_{\omega_i} = \sum_{\ell=0}^{\mathbf{N}_{\text{ref}}} \mu_\ell^{(i)} A^{(\ell)}$$

where the coefficients  $\mu_\ell^{(i)}$  are defined as follows: for  $\ell \geq 1$ ,  $\mu_\ell^{(i)} \in \{0, 1\}$  indicates whether a defect is present at the reference location  $\ell$  within the patch  $\omega_i$ . Since the defects are non-overlapping and

enter additively, the background weight satisfies  $\mu_0^{(i)} = 1 - \mathbf{N}_{\text{def}}^{(i)}$  with  $\mathbf{N}_{\text{def}}^{(i)}$  denoting the number of defects intersecting  $\omega_i$ . In particular, the coefficients satisfy

$$\sum_{\ell=0}^{\mathbf{N}_{\text{ref}}} \mu_{\ell}^{(i)} = 1.$$

This sum-constraint-one model holds for all defect models considered in this paper since the defects are fully localized in periodic  $\varepsilon$ -cells. Further details regarding the computations of  $\mu_{\ell}^{(i)}$  can be found at [14, 12], where we emphasize that no costly calculations are necessary to determine  $\mu_{\ell}^{(i)}$ .

Based on this representation, the exact local operator  $\mathcal{B}_i(A)$  is approximated by a linear combination of the precomputed reference local operators. We define the approximate local operator by

$$\tilde{\mathcal{B}}_i(A) = \sum_{\ell=0}^{\mathbf{N}_{\text{ref}}} \mu_{\ell}^{(i)} \mathcal{B}_i^{(\ell)}.$$

Finally, we obtain the offline-online preconditioner by replacing the exact local operators in the additive subspace decomposition by their offline-online approximations. Specifically, we define the operator

$$\tilde{\mathcal{B}}(A) := \mathcal{B}_0(A) + \sum_{i \geq 1} \tilde{\mathcal{B}}_i(A),$$

where the local operators  $\tilde{\mathcal{B}}_i(A)$  are defined by the online combination from above. The coarse operator  $\mathcal{B}_0(A)$  acts on the coarse space  $V_H$  and is assembled and applied exactly. The efficient computation of the  $\mathcal{B}_0(A)$  is discussed in Section 5.2. Since  $\dim V_H \ll \dim V_h$ , its computational cost is negligible compared to the patch-local solves. The operator  $\tilde{\mathcal{B}}(A)$  therefore preserves the additive structure of the exact subspace decomposition preconditioner, while avoiding the need to construct local operators for every realization of the coefficient. The idea is that  $\tilde{\mathcal{B}}(A)$  is an approximation of  $\mathcal{B}(A)$  and we will analyze the effect of this approximation via perturbation arguments in the next section.

**Remark 3.1.** It is possible to generalize the construction of the offline-online preconditioner to also include neighboring pairs of defects in the offline phase. While this would slightly increase the cost of the offline phase it would decrease the number of iterations needed for higher value of  $p$ , where neighboring pairs of defects occur more frequently.

## 4 Convergence analysis

In this section, we analyze the effect of the offline-online approximation introduced in Section 3 on the convergence of the preconditioned conjugate gradient method. We rely on the classical results from additive Schwarz theory. Our goal is to compare the exact subspace decomposition preconditioner with its offline-online approximation and to quantify the impact of the approximation on the spectral properties of the preconditioned operator. All operators and spaces used in this section are understood as defined in Section 2. In particular, we recall that  $\mathcal{L}(A) : V_h \rightarrow V_h'$  defines the stiffness operator associated with the bilinear form  $a(\cdot, \cdot)$ , and  $\mathcal{B}(A)$  and  $\tilde{\mathcal{B}}(A)$  denote the exact and approximate additive subspace decomposition preconditioners respectively.

### 4.1 Iteration by subspace decomposition

We first recall the spectral properties of the exact subspace decomposition preconditioner and the resulting PCG convergence, cf. [13, 5]. Recall that

$$\mathcal{B}(A) := \sum_{i=0}^{|\mathcal{N}|} \mathcal{B}_i(A), \quad \mathcal{P}(A) := \mathcal{B}(A) \circ \mathcal{L}(A)$$

where  $\mathcal{B}_i(A)$ ,  $i \geq 1$  are the (exact) local operators defined in Section 2.3.

**Lemma 4.1.** *For each  $i = 0, \dots, |\mathcal{N}|$ , the solution operator  $\mathcal{B}_i(A)$  satisfies the following property*

$$\langle g_1, \mathcal{B}_i(A)g_2 \rangle = \langle g_2, \mathcal{B}_i(A)g_1 \rangle \quad g_1, g_2 \in V_h'. \quad (4.1)$$

*Proof.* By the definition of  $\mathcal{B}_i(A)$ , we have  $\langle g_1, \mathcal{B}_i(A)g_2 \rangle = a(\mathcal{B}_i(A)g_1, \mathcal{B}_i(A)g_2)$ . Since the bilinear form  $a(\cdot, \cdot)$  is symmetric, we have  $a(\mathcal{B}_i(A)g_1, \mathcal{B}_i(A)g_2) = a(\mathcal{B}_i(A)g_2, \mathcal{B}_i(A)g_1) = \langle g_2, \mathcal{B}_i(A)g_1 \rangle$ , where we used the definition of  $\mathcal{B}_i(A)$  again in the last step.  $\square$

The next lemma follows immediately from Lemma 4.1 and the symmetry of the bilinear form, and therefore the proof is omitted.

**Lemma 4.2** (Symmetry of the local projections). *For each  $i = 0, \dots, |\mathcal{N}|$ , the operator  $\mathcal{P}_i(A) = \mathcal{B}_i(A) \circ \mathcal{L}(A)$  is symmetric with respect to the energy inner product, i.e.,*

$$a(\mathcal{P}_i(A)v, w) = a(v, \mathcal{P}_i(A)w) \quad \forall v, w \in V_h.$$

Note that Lemma 4.2 can also be proved directly using the variational characterization (2.5) of  $\mathcal{P}_i(A)$ .

Besides the symmetry, positive-definiteness of the operator  $\mathcal{P}(A)$  plays a decisive role. The latter is proved from two key properties of the subspace decomposition, which in our case have been proven, e.g. in [13]. The relevant result is the following.

**Proposition 4.3** (see Lemma 3.1 in [13]). *The operator  $\mathcal{P}(A) = \sum_{i=0}^{|\mathcal{N}|} \mathcal{P}_i(A)$  is symmetric. Under the stable decompositions, there exist constants  $C_1, C_2 > 0$ , independent of the mesh parameters and of the coefficient  $A$ , such that*

$$C_1 \|v\|_a^2 \leq a(\mathcal{P}(A)v, v) \leq C_2 \|v\|_a^2 \quad \forall v \in V_h. \quad (4.2)$$

The symmetry and the positive-definiteness of  $\mathcal{P}(A)$  allow us to apply the classical results from additive Schwarz theory (see, e.g., [13, 5]). In particular, the spectrum of  $\mathcal{P}(A)$  is uniformly bounded, i.e., the spectrum is contained in  $[C_1, C_2]$ , and the condition number of  $\mathcal{P}(A)$  is bounded by  $C_2/C_1$ . If  $u_h^{(k)}$  denotes the  $k$ -th iterate of the preconditioned conjugate gradient method applied to  $\mathcal{L}(A)u = f$  with a symmetric positive-definite preconditioner  $\mathcal{B}(A)$ , then the classical PCG theory yields the error estimate

$$\|u_h - u_h^{(k)}\|_a \leq 2 \left( \frac{\sqrt{\kappa} - 1}{\sqrt{\kappa} + 1} \right)^k \|u_h - u_h^{(0)}\|_a, \quad (4.3)$$

where  $\kappa$  denotes the condition number of  $\mathcal{P}(A)$ ; see e.g., [22].

## 4.2 Approximate preconditioner and perturbation framework

We now turn to the offline-online approximation introduced in Section 3. Recall that the approximate preconditioner is defined by

$$\tilde{\mathcal{B}}(A) := \mathcal{B}_0(A) + \sum_{i \geq 1} \tilde{\mathcal{B}}_i(A),$$

where the coarse operator  $\mathcal{B}_0(A)$  is assembled exactly and only the patch-local operator are approximated. The associated preconditioned operator is

$$\tilde{\mathcal{P}}(A) := \tilde{\mathcal{B}}(A) \circ \mathcal{L}(A).$$

We now want to show that this approximate preconditioned operator is also symmetric and, subsequently, determine bounds on its spectrum. In this way, we can guarantee that the error from the PCG solver with  $\tilde{\mathcal{B}}$  as a left-preconditioner is bounded and small. We first show the symmetry of  $\tilde{\mathcal{P}}(A)$  in the following following proposition.

**Proposition 4.4.** *For each realization of the coefficient  $A$ , the operator  $\tilde{\mathcal{P}}(A) : V_h \rightarrow V_h$  is symmetric with respect to the energy inner product  $a(\cdot, \cdot)$ , that is,*

$$a(\tilde{\mathcal{P}}(A)v, w) = a(v, \tilde{\mathcal{P}}(A)w) \quad \forall v, w \in V_h.$$

*Proof.* In order to prove the symmetry of  $\mathcal{P}(A)$ , for arbitrary  $v, w \in V_h$ , we compute

$$a(\tilde{\mathcal{P}}(A)v, w) = a(\tilde{\mathcal{B}}(A)\mathcal{L}(A)v, w) = \langle \mathcal{L}(A)\tilde{\mathcal{B}}(A)\mathcal{L}(A)v, w \rangle.$$

Since the stiffness operator  $\mathcal{L}(A)$  is defined via a symmetric bilinear form, we have

$$\langle \mathcal{L}(A)\tilde{\mathcal{B}}(A)\mathcal{L}(A)v, w \rangle = \langle \mathcal{L}(A)w, \tilde{\mathcal{B}}(A)\mathcal{L}(A)v \rangle.$$

Now recall that all  $\mathcal{B}_i(A)$  satisfy the property (4.1). Since each  $\tilde{\mathcal{B}}_i(A)$  for  $i \geq 1$  is a finite linear combination of such solution operators for reference coefficients, they inherit (4.1). As a consequence, we obtain this also for  $\tilde{\mathcal{B}}(A)$ . Therefore, together with the definition of  $\mathcal{L}(A)$ , we obtain

$$\langle \mathcal{L}(A)w, \tilde{\mathcal{B}}(A)\mathcal{L}(A)v \rangle = \langle \mathcal{L}(A)v, \tilde{\mathcal{B}}(A)\mathcal{L}(A)w \rangle = a(v, \tilde{\mathcal{P}}(A)w).$$

This proves that  $\tilde{\mathcal{P}}(A)$  is symmetric with respect to the energy inner product  $a(\cdot, \cdot)$ .  $\square$

The key idea is to interpret the offline-online approximation as a perturbation of the exact subspace decomposition preconditioner. More precisely, we compare the approximate operator  $\tilde{\mathcal{P}}(A)$  with the exact operator  $\mathcal{P}(A)$  by analyzing the perturbation

$$E(A) := \tilde{\mathcal{P}}(A) - \mathcal{P}(A)$$

To this end, we introduce the perturbation constant  $\eta$

$$\eta := \sup_{v \in V_h \setminus \{0\}} \frac{|a(E(A)v, v)|}{\|v\|_a^2}. \quad (4.4)$$

By construction,  $\eta = 0$  if all local operators are assembled exactly. The definition of  $\eta$  immediately implies that

$$|(E(A)v, v)| \leq \eta \|v\|_a^2. \quad (4.5)$$

**Theorem 4.5** (Stability of the offline-online preconditioner.). *Assume that the exact preconditioned operator  $\mathcal{P}(A)$  satisfies the spectral bounds (4.2)*

*and that the perturbation constant  $\eta$  defined in (4.4) satisfies  $\eta < C_1$ . Then the approximate preconditioned operator  $\tilde{\mathcal{P}}(A)$  satisfies*

$$(C_1 - \eta)\|v\|_a^2 \leq a(\tilde{\mathcal{P}}(A)v, v) \leq (C_2 + \eta)\|v\|_a^2 \quad \forall v \in V_h.$$

*In particular, the spectrum of  $\tilde{\mathcal{P}}(A)$  is contained in the interval  $[C_1 - \eta, C_2 + \eta]$ . Consequently, the condition number of the preconditioned operator  $\tilde{\mathcal{P}}(A) = \tilde{\mathcal{B}}(A)\mathcal{L}(A)$  satisfies*

$$\kappa(\tilde{\mathcal{P}}(A)) \leq \frac{C_2 + \eta}{C_1 - \eta}.$$

*Proof.* By definition of the perturbation operator  $E(A)$ , we have,

$$\tilde{\mathcal{P}}(A) = \mathcal{P}(A) + E(A).$$

Therefore, for any  $v \in V_h$ ,

$$a(\tilde{\mathcal{P}}(A)v, v) = a(\mathcal{P}(A)v, v) + a(E(A)v, v).$$

From the spectral bounds for the exact preconditioned operator  $\mathcal{P}(A)$ , cf. (4.2), and the bound of the perturbation term (4.5), we obtain

$$a(\tilde{\mathcal{P}}(A)v, v) \geq C_1\|v\|_a^2 - \eta\|v\|_a^2 = (C_1 - \eta)\|v\|_a^2, \quad \text{and} \quad a(\tilde{\mathcal{P}}(A)v, v) \leq C_2\|v\|_a^2 + \eta\|v\|_a^2 = (C_2 + \eta)\|v\|_a^2.$$

The assumption  $\eta < C_1$  ensures that the lower bound is strictly positive, and hence  $\tilde{\mathcal{P}}(A)$  is uniformly positive definite with respect to the energy inner product.

Since  $\tilde{\mathcal{P}}(A)$  is symmetric and positive definite, its spectrum is contained in the interval  $[C_1 - \eta, C_2 + \eta]$ , and therefore the condition number satisfies

$$\kappa(\tilde{\mathcal{P}}(A)) \leq \frac{C_2 + \eta}{C_1 - \eta}. \quad \square$$

Finally, note that  $\tilde{\mathcal{P}}(A) = \tilde{\mathcal{B}}(A) \circ \mathcal{L}(A)$  is exactly the operator governing the preconditioned conjugate gradient iteration for the system  $\mathcal{L}(A)u_h = f$ . Consequently, the above spectral bounds directly controls the convergence of the PCG method.

**Corollary 4.6** (PCG convergence). *Let  $u_h \in V_h$  denote the reference solution of  $\mathcal{L}(A)u = f$ , and let  $\tilde{u}_h^{(k)}$  be the  $k$ -th iterate of the preconditioned conjugate gradient method with preconditioner  $\tilde{\mathcal{B}}(A)$ . Under the assumptions of Theorem 4.5, the iterates satisfy*

$$\|u_h - \tilde{u}_h^{(k)}\|_A \leq 2 \left( \frac{\sqrt{\kappa(\tilde{\mathcal{P}}(A)) - 1}}{\sqrt{\kappa(\tilde{\mathcal{P}}(A)) + 1}} \right)^k \|u_h - \tilde{u}_h^{(0)}\|_A.$$

This estimate follows directly from the classical PCG convergence bound in (4.3), applied to the symmetric positive definite operator  $\tilde{\mathcal{P}}(A)$ .

Theorem 4.5 and Corollary 4.6 show that the offline-online approximation preserves the convergence properties of the exact subspace decomposition preconditioner as long as the perturbation constant  $\eta$  remains sufficiently small. In particular, the PCG convergence rate depends only on the perturbed spectral bounds and is therefore robust with respect to the fine-scale discretization. The size of  $\eta$  is governed by the quality of the offline-online approximation of the local operators  $\tilde{\mathcal{B}}_i(A)$ , which in turn depends on the localized structure of the defects and the restriction to a small set of reference coefficients. Quantitative insights into the constant  $\eta$  is presented numerically in Section 6. While  $\eta$  is defined abstractly at the operator level, its magnitude can be interpreted in practice by comparing the exact preconditioner  $\mathcal{B}(A)$  with its offline-online approximation  $\tilde{\mathcal{B}}(A)$ . In Section 6.3, we therefore report numerical experiments that measure the relative deviation  $\|(\mathcal{B} - \tilde{\mathcal{B}})r\|/\|\mathcal{B}r\|$  for random test vectors  $r$ .

To obtain an analytical estimate of the perturbation constant  $\eta$ , we analyze the difference between the operators. In particular, we consider the error operator  $E(A) = \mathcal{P}(A) - \tilde{\mathcal{P}}(A)$  and derive a bound in terms of patch local quantities. For simplicity, we omit the explicit dependency on  $A$  in the following.

**Proposition 4.7.** *Define for  $i \in \mathcal{N}$*

$$E_i := \max_{v \in V_h \setminus \{0\}} \frac{\|\sum_{\ell=0}^{M_{\text{ref}}} \mu_\ell^{(i)} A^{-1/2} (A^{(\ell)} - A) \nabla \mathcal{P}_i^{(\ell)} v\|_{L^2(\omega_i)}^2}{\|v\|_{a, \omega_i}^2}.$$

*Then, for any  $v \in V_h$ , it holds that*

$$\|(\mathcal{P} - \tilde{\mathcal{P}})v\|_a \leq C_{\text{overlap}} \left( \max_{i \in \mathcal{N}} E_i \right) \|v\|_a$$

*where  $C_{\text{overlap}}$  is the maximum possible patch overlap.*

*Proof.* Recall that  $\mathcal{B}_0$  and therefore also  $\mathcal{P}_0$  is computed exactly for any given  $A$ . Then we obtain that

$$\begin{aligned} \|(\mathcal{P} - \tilde{\mathcal{P}})v\|_a^2 &= (A \nabla (\mathcal{P} - \tilde{\mathcal{P}})v, \nabla (\mathcal{P} - \tilde{\mathcal{P}})v) = \sum_{i \geq 1} (A \nabla (\mathcal{P}_i - \tilde{\mathcal{P}}_i)v, \nabla e) \\ &\leq \sum_{i \geq 1} \|(\mathcal{P}_i - \tilde{\mathcal{P}}_i)v\|_{a, \omega_i} \|e\|_{a, \omega_i} \\ &\leq \left( \sum_{i \geq 1} \|(\mathcal{P}_i - \tilde{\mathcal{P}}_i)v\|_{a, \omega_i}^2 \right)^{1/2} \left( \sum_{i \geq 1} \|e\|_{a, \omega_i}^2 \right)^{1/2} \end{aligned} \quad (4.6)$$

where the last inequality is achieved by applying the Cauchy-Schwarz inequality. We hence estimate these terms separately. Note that the goal is to estimate  $(\mathcal{P}_i - \tilde{\mathcal{P}}_i)$  in terms of  $\|v\|_{a, \omega_i}$ , so that with the finite overlap of the patches, the final estimate will be independent from the number of patches. By the definition of  $\mathcal{P}_i$ ,  $\tilde{\mathcal{P}}_i$ , and  $A = \sum_{\ell=0}^{M_{\text{ref}}} \mu_\ell^{(i)} A^{(\ell)}$  on  $\omega_i$ , we have that

$$\|(\mathcal{P}_i - \tilde{\mathcal{P}}_i)v\|_{a, \omega_i}^2 = (A \nabla (\mathcal{P}_i - \tilde{\mathcal{P}}_i)v, \nabla (\mathcal{P}_i - \tilde{\mathcal{P}}_i)v) \\ =: \|w\|_{H_0^1(\omega_i)}^2$$

$$\begin{aligned}
&= (A\nabla v, \nabla w) - \sum_{\ell=0}^{N_{\text{ref}}} \mu_\ell^{(i)} (A\nabla \mathcal{P}_i^{(\ell)} v, \nabla w) \\
&= \sum_{\ell=0}^{N_{\text{ref}}} \mu_\ell^{(i)} (A^{(\ell)} \nabla v, \nabla w) - \sum_{\ell=0}^{N_{\text{ref}}} \mu_\ell^{(i)} (A\nabla \mathcal{P}_i^{(\ell)} v, \nabla w) \\
&= \sum_{\ell=0}^{N_{\text{ref}}} (\mu_\ell^{(i)} (A^{(\ell)} - A) \nabla \mathcal{P}_i^{(\ell)} v, \nabla w) \\
&= \sum_{\ell=0}^{N_{\text{ref}}} (\mu_\ell^{(i)} A^{-1/2} (A^{(\ell)} - A) \nabla \mathcal{P}_i^{(\ell)} v, A^{1/2} \nabla w).
\end{aligned}$$

Now inserting back for  $w$ , we get

$$\|(\mathcal{P}_i - \tilde{\mathcal{P}}_i)v\|_{a, \omega_i} \leq \left\| \sum_{\ell=0}^{N_{\text{ref}}} \mu_\ell^{(i)} A^{-1/2} (A^{(\ell)} - A) \nabla \mathcal{P}_i^{(\ell)} v \right\|_{L^2(\omega_i)}.$$

Therefore

$$\sum_{i \geq 1} \|(\mathcal{P}_i - \tilde{\mathcal{P}}_i)v\|_{a, \omega_i}^2 \leq \sum_{i \geq 1} E_i^2 \|v\|_{a, \omega_i}^2 \leq \left( \max_{i \in \mathcal{N}} E_i \right)^2 \sum_{i \geq 1} \|v\|_{a, \omega_i}^2 \quad (4.7)$$

Using that each  $x \in \Omega$  only belong at most to  $C_{\text{overlap}}$  patches, we deduce that

$$\sum_{i \geq 1} \|v\|_{a, \omega_i}^2 \leq C_{\text{overlap}} \|v\|_a^2 \quad (4.8)$$

Using this also for  $\|e\|_{a, \omega_i}^2$ , we get with (4.7) and (4.8) in (4.6) that

$$\|(\mathcal{P} - \tilde{\mathcal{P}})v\|_a \leq C_{\text{overlap}} \left( \max_{i \in \mathcal{N}} E_i \right) \|v\|_a. \quad \square$$

Note that  $E_i$  can be computed efficiently in the offline-online strategy similar to the upper bound  $E_T$  in [14], see also [6, 7].

## 5 Implementation aspects

In this section, we describe the practical realization of the offline-online subspace preconditioner introduced in Section 3. Here we explain how the operators  $\mathcal{B}_i$  and  $\mathcal{B}_0$  are assembled efficiently in practice. We also discuss cost, storage, and implementation remarks that are essential for large-scale Monte-Carlo simulations.

### 5.1 Practical realization of local operators

Recall that the local solution operator  $\mathcal{B}_i(A) : V_h' \rightarrow V_i$  is defined by

$$a(\mathcal{B}_i(A)g, w) = \langle g, w \rangle \quad \forall w \in V_i \quad (5.1)$$

where  $V_i := V_h \cap H_0^1(\omega_i)$ . In practice, this corresponds to solving a linear system on the fine-grid degrees of freedom associated with the patch  $\omega_i$ . Let  $R_i$  denote the restriction operator that extracts the free fine-scale degrees of freedom belonging to  $\omega_i$ . A detailed implementation of this restriction operator can be found in [8, Section 4]. Then the action of  $\mathcal{B}_i(A)$  on a vector  $g$  can be written as

$$\mathcal{B}_i(A)g = R_i^\top (K_i(A))^{-1} R_i g,$$

where  $K_i(A)$  is the patch-local stiffness matrix assembled with coefficient  $A$  and homogeneous Dirichlet conditions on  $\partial\omega_i$ . As we already discussed in Sections 2-3, direct construction of this  $\mathcal{B}_i(A)$  for every realization and every patch is computationally expensive. Therefore, instead of computing  $\mathcal{B}_i(A)$ , we

assemble the patch-local stiffness matrices corresponding to the reference coefficients  $A^{(\ell)}$  on  $\widehat{\omega}$ , and compute their reference factorizations  $\mathcal{B}_{\text{ref}}^{(\ell)}(A^{(\ell)})g$  for every  $\ell$ . These reference operators are computed once and stored. This is our offline phase. No information about a particular realization of the random coefficient is required at this stage.

In the online phase, for a given realization of the coefficient  $A(\cdot, \omega)$ , we loop over all interior patches  $\omega_i$ . Using the defect configuration within  $\omega_i$ , we first determine the weights  $\{\mu_\ell^{(i)}\}_{\ell=0}^{N_{\text{ref}}}$  by a simple sorting of the local defect cells into the corresponding reference positions. Then, we assemble the approximate local operator on  $\omega_i$  by a purely algebraic procedure

$$\widetilde{\mathcal{B}}_i(A) = \sum_{\ell=0}^{N_{\text{ref}}} \mu_\ell^{(i)} \mathcal{T}_i \mathcal{B}_{\text{ref}}^{(\ell)} \mathcal{T}_i^{-1},$$

where  $\mathcal{T}_i$  denotes the index permutation that maps the degrees of freedom of the reference patch to those of  $\omega_i$ . Importantly, no fine-scale linear systems are solved in the online phase; only linear combinations and index permutations are required.

## 5.2 Efficient construction of the coarse operator

Recall that  $V_0 = V_H$  and that the coarse operator  $\mathcal{B}_0(A) : V_h' \rightarrow V_H$  is defined by

$$a(\mathcal{B}_0(A)g, w_H) = \langle g, w_H \rangle \quad \forall w_H \in V_H.$$

On the discrete level, computing  $\mathcal{B}_0(A)g$  amounts to solving the coarse system

$$K_0(A)u_0 = g_0,$$

where  $K_0(A)$  is the stiffness matrix on the coarse mesh  $\mathcal{T}_H$  and  $g_0$  collects the duality pairings with the coarse basis functions. Since  $\dim V_H$  is small, solving this system is inexpensive. The main challenge is assembling  $K_0(A)$  efficiently for many realizations of the defect coefficient. This is achieved by an exact offline-online strategy at the coarse-element level. In the offline phase, we fix a reference coarse element  $\widehat{T}$  and construct reference coarse-element stiffness matrices  $\{K_{0,\widehat{T}}^{(\hat{\ell})}\}_{\hat{\ell}=0}^{N_{\text{ref}}}$  corresponding to the background coefficient and all single-defect positions  $\hat{\ell} = 1, \dots, N_{\text{ref}}$ . In the online phase, for each coarse element  $T \in \mathcal{T}_H$ , we determine coefficients  $\{\lambda_\ell^{(T)}\}$  such that

$$A|_T = \sum_{\hat{\ell}} \lambda_\ell^{(T)} A_{\widehat{T}}^{(\hat{\ell})},$$

and assemble

$$K_{0,T}(A) = \sum_{\hat{\ell}} \lambda_\ell^{(T)} K_{0,\widehat{T}}^{(\hat{\ell})}.$$

The global coarse stiffness matrix is then obtained by standard finite element assembly.

## 5.3 The algorithm

In this section we illustrate the offline-online algorithm of the additive preconditioner in Algorithm 1 that we can use in standard preconditioned conjugate gradient methods. We additionally remark on possible further implementation efficiency.

**Remark 5.1.** (Incremental representation) An equivalent representation of the coarse-element matrix in step (17) of Algorithm 1 is

$$K_{0,T}(A) = K_{0,\widehat{T}}^{(0)} + \sum_{q \in S_T} \left( K_{0,\widehat{T}}^{(q)} - K_{0,\widehat{T}}^{(0)} \right),$$

where  $S_T$  denotes the set of defect cells inside  $T$ . Both formulations are algebraically identical; the  $\lambda$ -representation is conceptually simpler, while the incremental form may reduce scaling costs.

---

**Algorithm 1** Offline-online construction of the additive preconditioner

---

- 1: **Input:** Background coefficient  $A_\varepsilon$ , defect coefficient  $B_\varepsilon$ , reference cell  $Q$ , right-hand side  $f$
- 2: Fix a reference patch  $\widehat{\omega}$  of the coarse mesh  $\mathcal{T}_H$ . ▷ Offline phase
- 3: Construct the family of reference patch coefficients  $\{A^{(\ell)}\}_{\ell=0}^{N_{\text{ref}}}$  on  $\widehat{\omega}$  and the family of reference coarse-element coefficients  $\{A^{(\hat{\ell})}\}_{\hat{\ell}=0}^{\hat{N}_{\text{ref}}}$  on a fixed reference coarse element  $\widehat{T} \subset \widehat{\omega}$ .
- 4: **for**  $\ell = 0, \dots, N_{\text{ref}}$  **do**
- 5:     Compute and store the reference patch operator  $\mathcal{B}_{\text{ref}}^{(\ell)} : \widehat{V}' \rightarrow \widehat{V}$  defined by

$$(A^{(\ell)} \nabla \mathcal{B}_{\text{ref}}^{(\ell)} g, \nabla w) = (g, w) \quad \forall w \in \widehat{V}.$$

- 6: **end for**
- 7: **for**  $\hat{\ell} = 0, \dots, \hat{N}_{\text{ref}}$  **do**
- 8:     Assemble and store the reference coarse-element stiffness matrix  $K_{0, \widehat{T}}^{(\hat{\ell})}$  associated with  $A^{(\hat{\ell})}$ .
- 9: **end for**
- 10: Precompute the canonical prolongation operator  $P : V_H \rightarrow V_h$ . ▷ End offline phase
- 11: **for** each realization of the coefficient  $A(\cdot, \omega)$  **do** ▷ Online phase
- 12:     **for** each interior patch  $\omega_i$  **do**
- 13:         Determine weights  $\{\mu_\ell^{(i)}\}_{\ell=0}^{N_{\text{ref}}}$  such that

$$A|_{\omega_i} = \sum_{\ell=0}^{N_{\text{ref}}} \mu_\ell^{(i)} A^{(\ell)}, \quad \sum_{\ell=0}^{N_{\text{ref}}} \mu_\ell^{(i)} = 1.$$

- 14:     Assemble the approximate local operator

$$\widetilde{\mathcal{B}}_i = \sum_{\ell=0}^{N_{\text{ref}}} \mu_\ell^{(i)} \mathcal{T}_i \mathcal{B}_{\text{ref}}^{(\ell)} \mathcal{T}_i^{-1},$$

where  $\mathcal{T}_i$  denotes the translation (index permutation) mapping the reference patch  $\widehat{\omega}$  to  $\omega_i$ .

- 15:     **end for**
- 16:     **for** each coarse element  $T \in \mathcal{T}_H$  **do**
- 17:         Determine weights  $\{\lambda_{\hat{\ell}}^{(T)}\}_{\hat{\ell}=0}^{\hat{N}_{\text{ref}}}$  and assemble the coarse-element stiffness contribution

$$K_{0, T}(A) = \sum_{\hat{\ell}=0}^{\hat{N}_{\text{ref}}} \lambda_{\hat{\ell}}^{(T)} K_{0, \widehat{T}}^{(\hat{\ell})}.$$

- 18:     **end for**
- 19:     Assemble the coarse operator

$$\mathcal{B}_0(A) = P \left( \sum_{T \in \mathcal{T}_H} K_{0, T}(A) \right)^{-1} P^T.$$

- 20:     Assemble the full preconditioner

$$\widetilde{\mathcal{B}}(A) = \mathcal{B}_0(A) + \sum_i \widetilde{\mathcal{B}}_i.$$

- 21:     Solve  $\mathcal{L}(A)u = f$  by PCG using  $\widetilde{\mathcal{B}}(A)$  as a left preconditioner.
  - 22: **end for**
- 

**Remark 5.2.** (Symmetry reduction) The offline cost for the coarse operator  $\mathcal{B}_0$  can be further reduced by exploiting geometric symmetries of the coarse element. Defect locations that are symmetry-equivalent lead to stiffness matrices that differ only by permutation of degrees of freedom. Thus, only one representative per symmetry class needs to be stored.

**Remark 5.3.** In principle, similar symmetry arguments apply to patch-local operators. However, due to the overlap of patches and the larger local dimensions, the required permutation logic is significantly more complex. For this reason, symmetry reduction is easily applicable only at the coarse level.

## 5.4 Run-time complexity

A natural benchmark for any approximate preconditioning strategy is the preconditioner based on the exact coefficient of the realization. This typically shows the best performances but can be too costly when many realizations must be solved. In the rare-defect regime considered here, an equally natural baseline is to construct a single preconditioner from the defect-free background coefficient and reuse it across all samples. When most realizations are close to the background, this approach can be effective while essentially eliminating the setup cost. The proposed offline-online strategy is designed to retain much of the accuracy of the sample-dependent construction while amortizing expensive local computation across samples.

Therefore, in this section, we compare the computational complexity of the proposed offline-online domain decomposition (OO-DD) preconditioner (in Algorithm 1) against these two baselines: (i) Direct-DD, i.e., the exact sample-dependent approach, and (ii) ND-DD, the “no-defect” approach, where the preconditioner is constructed once from the defect-free background and reused for all samples. The Direct-DD and OO-DD preconditioners share the same algebraic structure, differing only in the use of exact versus offline-online approximated local patch operators.

All methods are used as preconditioners in a standard preconditioned conjugate gradient (PCG) solver for the discrete linear system  $\mathcal{L}(A)u_h = f$ . Throughout the discussion, we focus on the cost of constructing and applying the preconditioner. The per-iteration cost of PCG, consisting of one fine-scale matrix-vector product and one application of the preconditioner, is comparable for all three methods and is therefore treated separately.

We assume a scale separation  $h \leq \varepsilon < H$ , where the fine mesh resolves all microscale features of the coefficient. The coarse mesh  $\mathcal{T}_H$  is assumed to be aligned with the periodic background coefficient. We consider vertex-centered patches with fixed overlap and layer size. The total number of interior patches satisfies  $N_p \sim H^{-d}$ , up to a constant depending only on the mesh connectivity. In the following, we therefore do not distinguish between the number of coarse elements and the number of patches, as these quantities are of the same order.

For simplicity, we only introduce the following representative costs.  $T_{\text{patch}}$ : cost of solving one fine-scale local problem on a patch;  $T_{\text{comb}}$ : cost of forming a linear combination of precomputed patch operators;  $T_{\text{PCG}}$ : cost of one PCG iteration. At the theoretical level, all patch-level solves involve matrices of comparable size and structure, so that a single representative cost  $T_{\text{patch}}$  is sufficient. Moreover, we denote  $k^D$ ,  $k^{\text{ND}}$ , and  $k^{\text{OO}}$  to be the number of PCG iterations required to reduce the residual below a prescribed stopping tolerance for the Direct-DD, ND-DD, and OO-DD preconditioners, respectively. Throughout the comparison, the tolerance is assumed to be fixed and identical for all methods. We further let  $N_{\text{samp}}$  be the number of random samples used.

For the Direct-DD method, the local operators are assembled exactly for each realization of the coefficient. There is no offline phase. For each sample coefficient, one must solve a local fine-scale problem on every patch resulting in a per sample online cost  $N_p T_{\text{patch}}$ . The total cost for  $N_{\text{samp}}$  samples is therefore

$$T^D \sim N_{\text{samp}} (N_p T_{\text{patch}} + k^D T_{\text{PCG}}).$$

In the ND-DD method, the preconditioner is constructed using only the periodic background coefficient  $A_\varepsilon$  and reused unchanged for all samples. Due to periodicity and translation invariance, all interior patches are equivalent. Consequently, the local operators need to be computed only once on a single reference patch and can then be reused by translation. This suggests one time offline cost  $T_{\text{patch}}$  and zero per sample online cost. The total cost is therefore

$$T^{\text{ND}} \sim T_{\text{patch}} + N_{\text{samp}} (k^{\text{ND}} T_{\text{PCG}}).$$

In the proposed OO-DD method, a small number of reference patch operators corresponding to different single-defect configurations are computed offline. In the online phase, the local operators for a given sample are obtained by linear combinations of these reference operators. No local fine-scale solves are required online. Hence, the one-time offline cost is  $N_{\text{ref}} T_{\text{patch}}$ , while the per-sample online cost is  $N_p T_{\text{comb}}$ . Here,  $N_{\text{ref}}$  denotes the number of reference coefficients. The total cost is therefore

$$T^{\text{OO}} \sim N_{\text{ref}} T_{\text{patch}} + N_{\text{samp}} (N_p T_{\text{comb}} + k^{\text{OO}} T_{\text{PCG}}).$$

To understand when the OO-DD is advantageous over the other two methods, one may consider

the break-even number of samples  $N_{\text{samp}}^*$ . With respect to the Direct-DD, equating  $T^{\text{OO}} = T^{\text{D}}$  yields

$$N_{\text{samp}}^* = \frac{N_{\text{ref}} T_{\text{patch}}}{N_{\text{p}} (T_{\text{patch}} - T_{\text{comb}}) + (\mathbf{k}^{\text{D}} - \mathbf{k}^{\text{OO}}) T_{\text{PCG}}}.$$

Since  $T_{\text{patch}} \gg T_{\text{comb}}$ , the denominator is large and the break-even number of samples is typically small. Similarly, with respect to ND-DD, equating  $T^{\text{OO}} = T^{\text{ND}}$  gives

$$N_{\text{samp}}^* = \frac{(N_{\text{ref}} - 1) T_{\text{patch}}}{(\mathbf{k}^{\text{ND}} - \mathbf{k}^{\text{OO}}) T_{\text{PCG}} - N_{\text{p}} T_{\text{comb}}}.$$

Here, the offline-online method becomes advantageous once the reduction in iteration counts is sufficient to compensate for the additional offline cost.

**Remark 5.4** (Asymptotic comparison). We provide a coarse asymptotic comparison of the three methods to highlight their dominant cost contributions. We denote by  $n_{\text{loc}}$  the dimension of the local finite element space on a single patch, and  $N_H := H^{-d}$  the total number of coarse elements. Let  $C_{\text{loc}}(n_{\text{loc}})$  and  $C_{\text{comb}}(n_{\text{loc}})$  be the cost of solving one local problem exactly, and the cost of forming a linear combination of precomputed local factorizations respectively. In all three methods, the coarse operator is assembled element-wise with linear complexity  $\mathcal{O}(N_H)$ . Since this cost is of lower order compared to the local patch contributions, it is omitted in the following comparison. In the Direct-DD method, all local problems are solved independently for each realization. The dominant cost therefore scales as  $\mathcal{O}(N_{\text{samp}} N_{\text{p}} C_{\text{loc}}(n_{\text{loc}}))$ , which grows linearly with both the number of samples and patches. In the ND-DD method, all local operators are constructed only once for the background coefficient and reused unchanged for all samples. The setup cost is therefore  $\mathcal{O}(C_{\text{loc}}(n_{\text{loc}}))$ , while the per-sample cost arises solely from the PCG iteration with a fixed preconditioner, and scales as  $N_{\text{samp}} \mathcal{O}(k^{\text{ND}} n_h)$ , where  $n_h$  the number of fine-scale degrees of freedom. In practice, this iteration count may increase significantly in the presence of strong defects or high contrast. In the OO-DD method, only  $N_{\text{ref}}$  reference patch problems are solved exactly in an offline stage. The corresponding setup cost is therefore  $\mathcal{O}(N_{\text{ref}} C_{\text{loc}}(n_{\text{loc}}))$ . In the online stage, the local operators are obtained by recombination of the precomputed reference data. The per-sample cost is thus  $N_{\text{samp}} \mathcal{O}(N_{\text{p}} C_{\text{comb}}(n_{\text{loc}}))$ , where typically  $C_{\text{comb}}(n_{\text{loc}}) \ll C_{\text{loc}}(n_{\text{loc}})$ .

If the local patch problems are solved by direct factorization on spaces of dimension  $n_{\text{loc}}$ , then  $C_{\text{loc}}(n_{\text{loc}}) = \mathcal{O}(n_{\text{loc}}^3)$ . Alternatively, if the local problems are solved approximately using optimal methods, one may assume  $C_{\text{loc}}(n_{\text{loc}}) = \mathcal{O}(n_{\text{loc}})$ . The recombination cost  $C_{\text{comb}}(n_{\text{loc}})$  depends on the chosen implementation but is always of lower order. In all cases, the qualitative comparison between the three methods remains unchanged.

The three preconditioners therefore represent different trade-offs. The Direct-DD method provides the smallest iteration numbers and thus the fastest convergence per sample, but at the price of the largest per-sample setup cost. The ND-DD method is computationally the cheapest in terms of setup, since the preconditioner is reused for all samples, but this advantage is often outweighed by a substantial increase in iteration numbers when defects are present. The OO-DD method balances these two extremes: its offline stage is more expensive than that of the ND-DD, but this cost is averaged over many samples, while its per-sample setup is much cheaper than that of the Direct-DD and its iteration numbers are typically close to those of the Direct-DD. Hence, for large Monte-Carlo simulations, the OO-DD preconditioner provides the most favorable compromise between computational cost and convergence speed. The numerical experiments in Section 6 underline this behavior and illustrate the practical relevance of the offline-online strategy.

**Remark 5.5** (Storage and parallelization). In the OO-DD method, all offline data are stored on a single reference patch and reused across the domain by translation, permutation, and symmetry arguments. The dominant offline memory consumption is due to the patch-local offline data associated with the  $N_{\text{ref}}$  reference defect configurations. Under an optimal setup,  $\text{Mem}_{\text{off}} = \Theta(N_{\text{ref}} n_{\text{loc}})$ . In addition, a small dictionary of reference coarse element blocks is stored, corresponding to a fixed number of symmetry classes. Since this contribution is independent of  $h$ ,  $H$ , and the number of samples, this storage memory is asymptotically negligible. Both the offline loop over reference configurations and the online loops over patches and coarse elements can be completely parallelized.

## 6 Numerical Experiments

In this section, we investigate the practical performance of the proposed OO-DD preconditioner. All experiments are conducted in two spatial dimensions on the unit domain  $D = [0, 1]^2$  with homogeneous Dirichlet boundary conditions. The goal of the experiments is threefold: (i) to assess the accuracy of the OO-DD preconditioner in the presence of random defects, (ii) to compare its efficiency with the Direct-DD and the ND-DD in terms of PCG iteration counts, and (iii) to demonstrate that the observed behavior persists across different defect geometries.

We consider the diffusion problem (2.1) discretized using  $Q_1$  finite elements on a fine mesh  $\mathcal{T}_h$  that resolves all microscale features of the coefficient. A nested coarse mesh  $\mathcal{T}_H$  is used to define the subspace decomposition. The meshes are aligned with the periodic background coefficient and satisfy  $h \leq \varepsilon < H$ . Throughout the experiments, we use the fixed patch size introduced in Section 2.2, namely vertex centered patches consisting of one layer of coarse elements. Unless stated otherwise, the right-hand side is chosen as

$$f(x, y) = \sin(\pi x) \sin(\pi y).$$

We have additionally verified all implementations for the constant right-hand side  $f \equiv 1$ , with no qualitative changes in the observed behavior. A direct finite element solution on the fine mesh  $\mathcal{T}_h$  is used as a reference solution for all accuracy comparisons.

We compare the proposed OO-DD preconditioner with the two standard preconditioning strategies introduced in Section 5.4 both within the same subspace-decomposition framework: Direct-DD and ND-DD preconditioners. In the following experiments, we report convergence behavior and average PCG iteration counts for varying defect probability, contrast, and defect geometry. These quantities serve as practical indicators for the robustness and efficiency of the respective preconditioners.

In all cases, the resulting linear systems are solved using the preconditioned conjugate gradient method as implemented in `scipy.sparse.linalg.cg` package, with a fixed relative residual tolerance of  $10^{-6}$  and a per sample maximum iteration count 200. Unless stated otherwise, we use the discretization parameters  $h = 2^{-7}$ ,  $\varepsilon = 2^{-5}$ , and  $H = 2^{-4}$ . All experimental results are averaged over 150 independent Monte-Carlo realizations of the coefficient. All experiments discussed in this section are fully reproducible. The corresponding code and data are publicly available at [11].

### 6.1 Random inclusion model

We first consider the random erasure model introduced in (2.2) and depicted in Figure 1.1, where defect inclusions of fixed shape are activated independently with probability  $p$ . Figures 6.1 and 6.2 summarize the performance of the three preconditioners for increasing defect probability and contrast.

Figure 6.1 reports the average number of PCG iterations as a function of the defect probability  $p$  for contrasts  $\beta/\alpha = 10, 100$ , and 500 (from left to right). For all tested configurations, the PCG method converges for all three preconditioners across all samples. Among the three methods, the Direct-DD preconditioner consistently yields the smallest number of iterations, as expected, since all local patch operators are assembled exactly for each realization of the coefficient. In contrast, the ND-DD preconditioner exhibits a substantial increase in iteration counts as the defect probability  $p$  increases and, in particular, as the contrast  $\beta/\alpha$  becomes large. This behavior reflects the growing mismatch between the defect-free preconditioner and the true operator when defects become more frequent and stronger.

The vertical bars indicate the statistical variation of the iteration counts after removing outlier samples. While ND-DD exhibits the largest variability across samples, the proposed OO-DD preconditioner shows significantly smaller variations and iteration counts that remain close to those of Direct-DD over the full range of defect probabilities. Although a mild increase in the number of iterations can be observed as  $p$  grows, the overall behavior demonstrates that the offline-online approximation successfully captures the dominant local effects induced by the defects.

Figure 6.2 illustrates the convergence histories of the PCG method measured in terms of the root-mean-square error (RMSE) in the energy norm for three given defect probabilities and contrast of  $\beta/\alpha = 500$ . For all three preconditioners, the energy-norm error decreases steadily with the iteration count, indicating consistent convergence of the method. The convergence curves further highlight clear qualitative differences between the preconditioners. The ND-DD preconditioner exhibits significantly slower decay of the energy error, whereas the proposed OO-DD preconditioner closely follows the convergence behavior of the Direct-DD method across all tested defect probabilities.

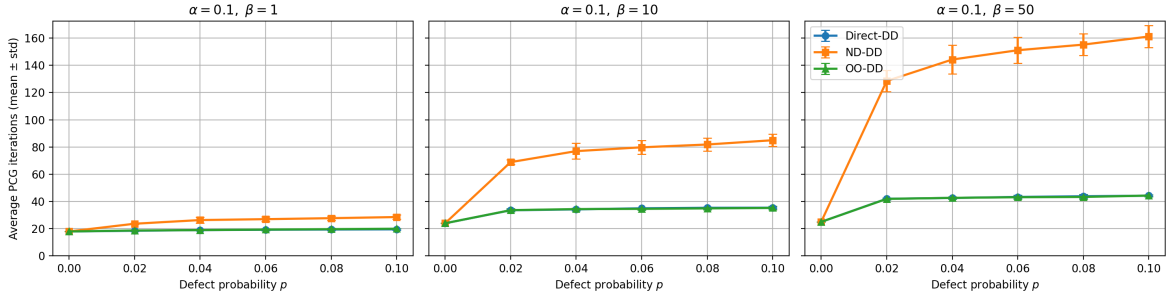


Figure 6.1: Random erasure model: the average PCG iteration counts against varying defect probabilities for defect contrasts  $\beta/\alpha = 10, 100$  and  $500$  (left to right) respectively.

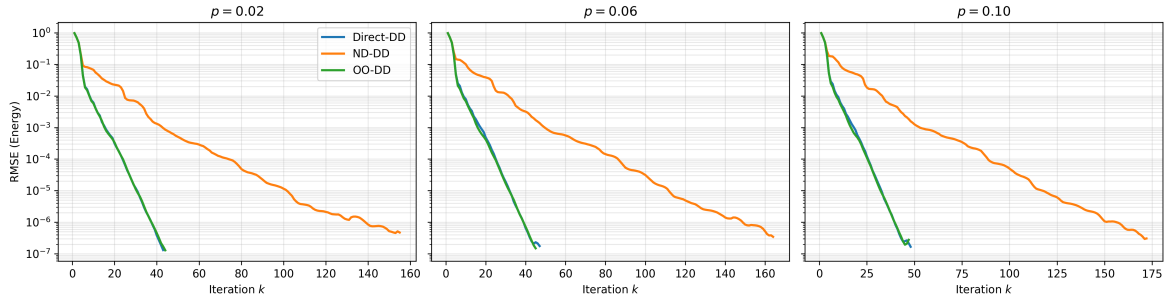


Figure 6.2: Random erasure model: the RMSE in the energy norm vs iteration count for defect probabilities  $p = 0.02, 0.06$  and  $0.10$  (left to right) respectively at  $\beta/\alpha = 500$ .

## 6.2 Other defect models

In the experiments, apart from the random erasure model depicted in Figure 1.1, we additionally consider two further random defect models which we introduce as an L-shape defect model [Figure 6.3 (left)] and a shifted defect model [Figure 6.3 (right)]. These models introduce different levels of geometric complexity and, they therefore serve to assess the robustness of the preconditioners with respect to changes in defect shape and spatial localization. Both models still fit into the general framework of (2.2) modifying only the local defect geometry encoded in  $B_\varepsilon$ .

### L-shaped random defect model

In the L-shaped model illustrated in Figure 6.3 (left), the defect geometry breaks rotational symmetry but distributes the coefficient perturbation over a larger portion of the local patch compared to the compact square inclusions considered previously.

For all tested defect probabilities and contrasts, the PCG method once again converges for all three preconditioners. An interesting observation in Figure 6.4 is that the ND-DD preconditioner exhibits smaller iteration counts for the L-shaped defect model than for the square inclusion model we observed in Figure 6.1. This behavior can be explained by the spatial distribution of the defect. While the square inclusion introduces a compact and strongly localized perturbation of the coefficient, the L-shaped defect distributes the same contrast over a larger region of the patch. As a result, the deviation of the true local operator from the defect-free background operator is less pronounced, leading to a smaller spectral mismatch and improved convergence of ND-DD. In contrast, the Direct-DD and OO-DD preconditioners are largely insensitive to this effect, as both methods explicitly account for the local defect structure. Consequently, their iteration counts remain comparable between the inclusion and L-shaped models.

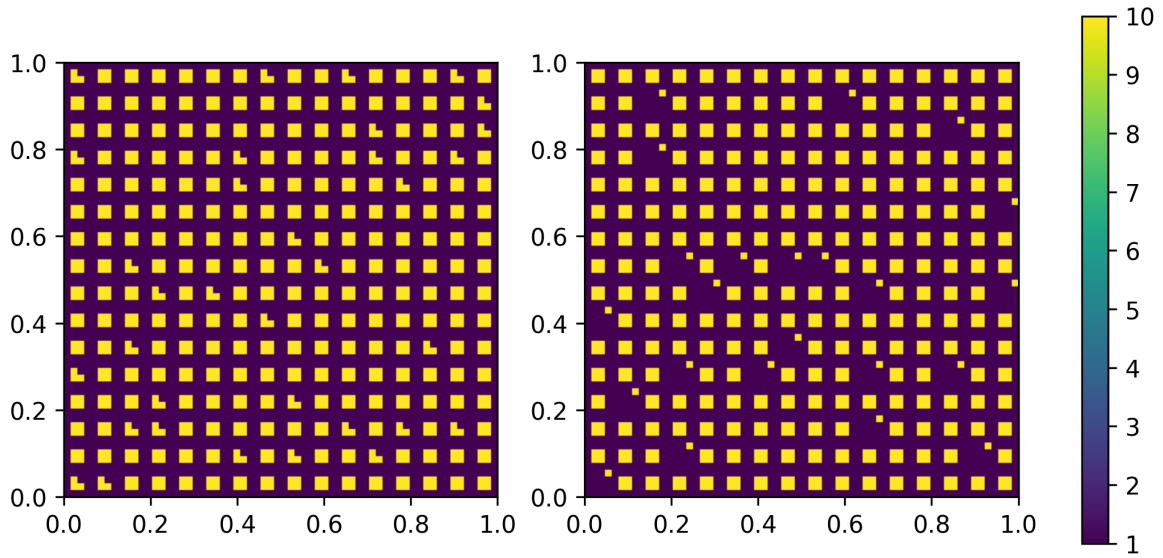


Figure 6.3: The random defect L-shape (left) and shift (right) coefficients with  $\alpha = 1$ ,  $\beta = 10$ ,  $p = 0.1$ ,  $\varepsilon = 2^{-5}$  and  $h = 2^{-9}$ .

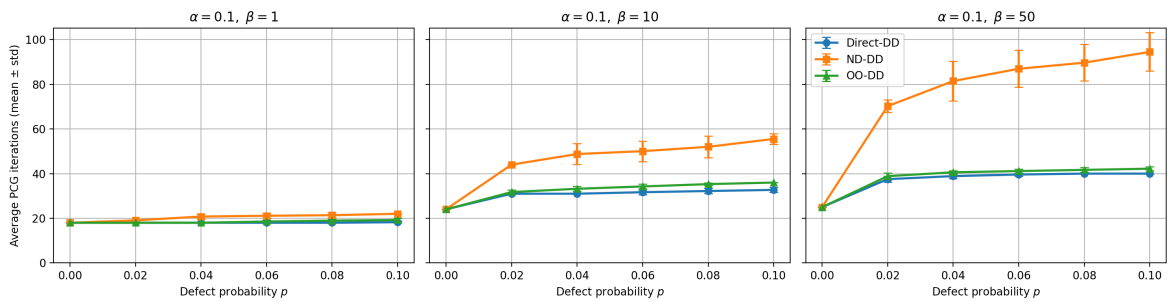


Figure 6.4: L-shaped random defect model: the average PCG iteration counts against varying defect probabilities for defect contrasts  $\beta/\alpha = 10, 100$  and  $500$  (left to right) respectively.

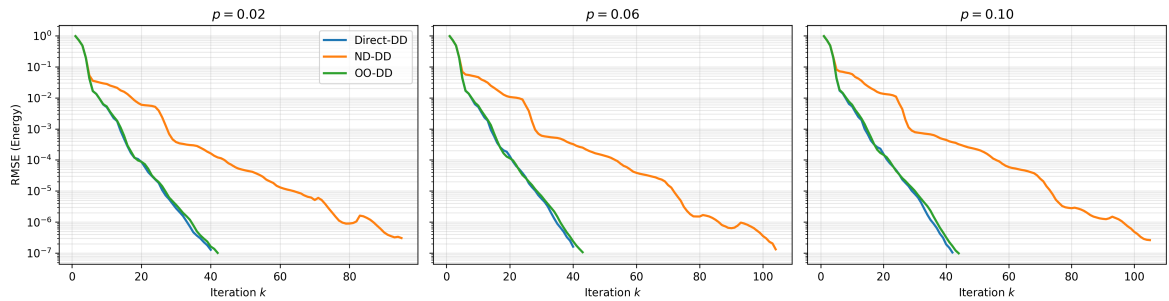


Figure 6.5: L-shaped random defect model: the RMSE in the energy norm vs iteration count for defect probabilities  $p = 0.02, 0.06$  and  $0.10$  (left to right) respectively at  $\beta/\alpha = 500$ .

### Shifted random defect model

We finally consider the random defect shifted model shown in Figure 6.3 (right), which represents the most challenging test case among the considered defect configurations. In contrast to the previous models, the defect is no longer centered within the  $\varepsilon$ -cell, although its fine-scale structure is preserved. This modification breaks the symmetry implicitly exploited by the ND-DD preconditioner.

Figure 6.6 reports the average number of PCG iterations of the converged samples. For smaller defect contrast e.g.  $\beta/\alpha = 10$ , all methods converged even with a clearly increased number of iterations. At a contrast  $\beta/\alpha = 100$ , the Direct-DD preconditioner remains robust for all tested defect probabilities, converging for all samples with only a mild increase in iteration counts. Similarly, the proposed OO-DD preconditioner converges for all samples across the full range of defect probabilities, with the average iteration count exhibiting an increase as the defect probability grows. However, for higher contrast, in particular at  $\beta/\alpha = 100$ , the ND-DD preconditioner exhibits a severe loss of robustness. Already for small defect probabilities, convergence within the prescribed maximum of 200 PCG iterations is observed only for a small fraction of the samples. More precisely, at defect probability  $p = 0.02$ , only 10.67% of all samples converged in 200 iterations. For moderate defect probabilities, no convergence is achieved within this iteration limit. As a consequence, iteration counts for ND-DD are not reported beyond this regime.

The energy-norm RMSE convergence histories in Figure 6.7 further confirm these observations. While the OO-DD preconditioner shows a stable and monotone decay of the energy error, the error reduction in ND-DD preconditioner is much slower and the error does not fall below the prescribed tolerance within the maximum of 200 iterations.

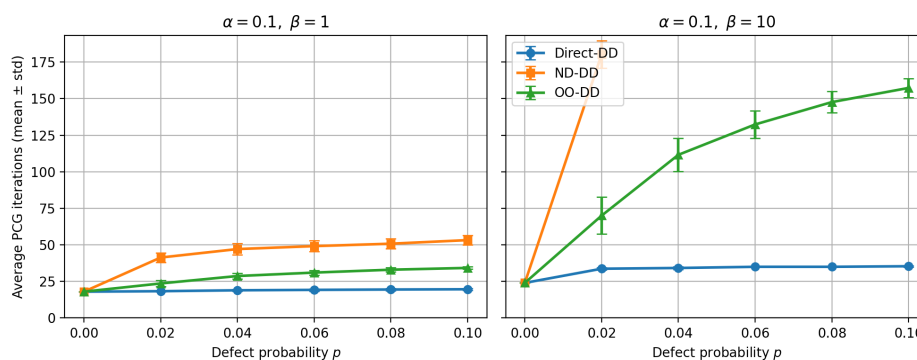


Figure 6.6: Shifted random defect model: the average PCG iteration counts against varying defect probabilities for defect contrasts  $\beta/\alpha = 10$  and 100 (left to right) respectively.

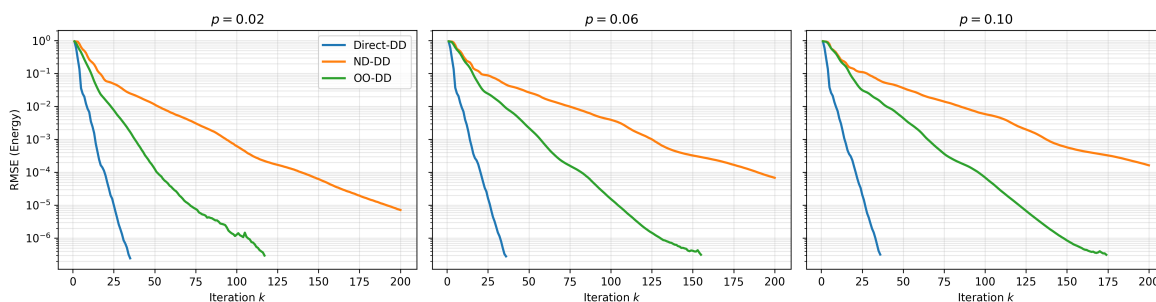


Figure 6.7: Shifted random defect model: the RMSE in the energy norm vs iteration count for defect probabilities  $p = 0.02, 0.06$  and  $0.10$  (left to right) respectively at  $\beta/\alpha = 100$ .

The numerical results across all defect models are fully consistent with the complexity analysis presented in Section 5. While the Direct-DD preconditioner yields the smallest iteration counts, its high per-sample cost due to fine-scale patch solves makes it computationally expensive in multi-sample settings. The ND-DD approach, despite its minimal setup cost, lacks robustness once defect symmetry/centering is violated or considered at higher defect contrast, and therefore fails in more challenging regimes. In contrast, the OO-DD preconditioner achieves robust convergence for all considered defect configurations with iteration counts close to those of Direct-DD, while incurring only inexpensive online recombination costs. These observations confirm that OO-DD provides the intended balance between robustness and computational efficiency predicted by the theoretical analysis.

### 6.3 Experimental $\mathcal{B}$ - $\tilde{\mathcal{B}}$ comparison

To complement the iteration-count results, we include a direct experimental comparison of the exact subspace preconditioner  $\mathcal{B}$  and its offline-online approximation  $\tilde{\mathcal{B}}$ . The purpose of this experiment is to quantify how accurately the offline-online construction reproduces the exact preconditioner at the operator level, and to contrast this behavior with the no-defect preconditioner.

For a fixed realization of the coefficient, we compute the exact operator  $\mathcal{B}$  (Direct-DD), the offline-online approximation  $\tilde{\mathcal{B}}$  (OO-DD), and the no-defect operator  $\mathcal{B}(A_0)$  (ND-DD). We measure the relative deviation using a random test vector  $r$ ,

$$\frac{\|(\mathcal{B} - \tilde{\mathcal{B}})r\|_2}{\|\mathcal{B}r\|_2},$$

where  $\tilde{\mathcal{B}}$  denotes either  $\tilde{\mathcal{B}}$  or  $\mathcal{B}(A_0)$ . The reported values are obtained by computing the RMSE of this relative deviation across all samples.

Figure 6.8 shows the resulting relative deviations for the random inclusion model for varying defect probabilities. For both methods mean relative deviation increase as  $p$  increases, reflecting the growing deviation of the coefficient from its approximation as more defects come into the play. However, the OO-DD preconditioner  $\tilde{\mathcal{B}}$  remains consistently much closer to the Direct-DD preconditioner  $\mathcal{B}$  than the ND-DD preconditioner  $\mathcal{B}(A_0)$  across the entire range of the considered defect probabilities. This behavior is consistent with the perturbation framework developed in Section 4 and explains why the convergence of OO-DD remains much closer to that of Direct-DD, whereas ND-DD deteriorates more rapidly.

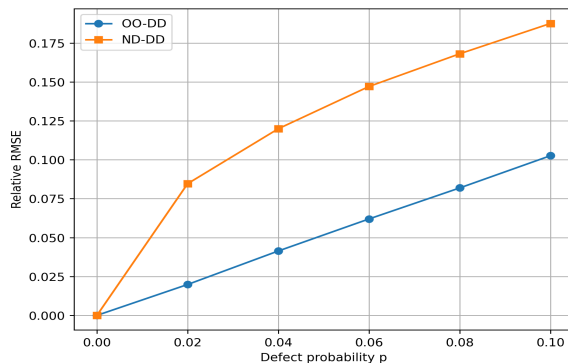


Figure 6.8: The operator behavior for varying defect probabilities in random inclusion model with contrast  $\beta/\alpha = 500$ .

## 7 Conclusion

In this work, we proposed and analyzed a two-level domain decomposition preconditioner for diffusion problems with localized random defects. The method is based on a subspace decomposition framework in which expensive fine-scale patch solves are computed in an offline stage and reused in the online stage through linear combinations of reference operators corresponding to single-defect configurations.

From a theoretical perspective, we derived perturbation-based bounds that quantify the effect of replacing exact local operators by offline-online approximations. These results indicate that the spectral properties of the preconditioned system degrade only moderately when the defect structure is well captured by the chosen reference space. A detailed run-time complexity analysis further demonstrated that, beyond a small break-even number of samples, the proposed method is expected to be significantly more efficient than direct domain decomposition approaches.

Extensive numerical experiments in two dimensions confirmed these theoretical findings. Across a range of defect probabilities, contrasts, and geometries, the OO-DD preconditioner consistently achieved convergence behavior close to that of the exact Direct-DD method while substantially reducing the per-sample computational cost. In particular, for shifted defect configurations that break defect centering, the ND-DD preconditioner was observed to lose convergence of the PCG solver, whereas the

OO-DD method remained fully convergent. Overall, the proposed offline-online strategy offers a robust and efficient preconditioning approach for multi-query diffusion problems with localized defects. Future work includes adaptive selection of reference defect configurations and extensions of the reference space to include multiple and overlapping defect configurations.

## Acknowledgments

This research is funded by the Deutsche Forschungsgemeinschaft (DFG, German Research Foundation) under project number 496556642. BV additionally acknowledges support from the Deutsche Forschungsgemeinschaft (DFG, German Research Foundation) under Germany’s Excellence Strategy – EXC-2047/1 – 390685813. AM acknowledges support from the Swedish Research Council, project number 2023-03258 VR. The authors would also like to thank the Hausdorff Institute for Mathematics (HIM), Bonn, for its hospitality, where part of this work was completed during the trimester program “Computational multifidelity, multilevel, and multiscale methods”.

## References

- [1] A. Anantharaman and C. Le Bris. Elements of mathematical foundations for numerical approaches for weakly random homogenization problems. *Commun. Comput. Phys.*, 11(4):1103–1143, 2012.
- [2] A. Bespalov, D. Loghin, and R. Youngnoi. Truncation preconditioners for stochastic Galerkin finite element discretizations. *SIAM J. Sci. Comput.*, 43(5):S92–S116, 2021.
- [3] A. A. Contreras, P. Mycek, O. P. Le Maître, F. Rizzi, B. Debusschere, and O. M. Knio. Parallel domain decomposition strategies for stochastic elliptic equations Part B: Accelerated Monte Carlo sampling with local PC expansions. *SIAM J. Sci. Comput.*, 40(4):C547–C580, 2018.
- [4] O. G. Ernst, C. E. Powell, D. J. Silvester, and E. Ullmann. Efficient solvers for a linear stochastic Galerkin mixed formulation of diffusion problems with random data. *SIAM J. Sci. Comput.*, 31(2):1424–1447, 2008/09.
- [5] M. Görtz, F. Hellman, and A. Målqvist. Iterative solution of spatial network models by subspace decomposition. *Math. Comp.*, 93(345):233–258, 2024.
- [6] F. Hellman, T. Keil, and A. Målqvist. Numerical upscaling of perturbed diffusion problems. *SIAM J. Sci. Comput.*, 42(4):A2014–A2036, 2020.
- [7] F. Hellman and A. Målqvist. Numerical homogenization of elliptic PDEs with similar coefficients. *Multiscale Model. Simul.*, 17(2):650–674, 2019.
- [8] F. Hellman, A. Målqvist, and M. Mosquera. Well-posedness and finite element approximation of mixed dimensional partial differential equations. *BIT*, 64(1):Paper No. 2, 22, 2024.
- [9] C. Jin and X.-C. Cai. A preconditioned recycling GMRES solver for stochastic Helmholtz problems. *Commun. Comput. Phys.*, 6(2):342–353, 2009.
- [10] C. Jin, X.-C. Cai, and C. Li. Parallel domain decomposition methods for stochastic elliptic equations. *SIAM J. Sci. Comput.*, 29(5):2096–2114, 2007.
- [11] D. Kolombage. offline-online-preconditioning: preprint version. software, <https://doi.org/10.5281/zenodo.18940922>, 2026.
- [12] D. Kolombage and B. Verfürth. Offline-online approximation of multiscale eigenvalue problems with random defects. *ESAIM Math. Model. Numer. Anal.*, 59(4):2055–2079, 2025.
- [13] R. Kornhuber and H. Yserentant. Numerical homogenization of elliptic multiscale problems by subspace decomposition. *Multiscale Model. Simul.*, 14(3):1017–1036, 2016.
- [14] A. Målqvist and B. Verfürth. An offline-online strategy for multiscale problems with random defects. *ESAIM Math. Model. Numer. Anal.*, 56(1):237–260, 2022.

- [15] O. Pembery. *The Helmholtz equation in heterogeneous and random media: analysis and numerics*. Phd thesis, University of Bath, 2020.
- [16] C. E. Powell and H. C. Elman. Block-diagonal preconditioning for spectral stochastic finite-element systems. *IMA J. Numer. Anal.*, 29(2):350–375, 2009.
- [17] C. E. Powell and E. Ullmann. Preconditioning stochastic Galerkin saddle point systems. *SIAM J. Matrix Anal. Appl.*, 35(1):314–315, 2014.
- [18] A. Quarteroni and A. Valli. *Domain decomposition methods for partial differential equations*. Numerical Mathematics and Scientific Computation. The Clarendon Press, Oxford University Press, New York, 1999. Oxford Science Publications.
- [19] J. F. Reis, O. P. Le Maître, P. M. Congedo, and P. Mycek. Stochastic preconditioning of domain decomposition methods for elliptic equations with random coefficients. *Comput. Methods Appl. Mech. Engrg.*, 381:Paper No. 113845, 29, 2021.
- [20] W. Subber and A. Sarkar. Domain decomposition methods of stochastic PDEs. In *Domain decomposition methods in science and engineering XX*, volume 91 of *Lect. Notes Comput. Sci. Eng.*, pages 191–198. Springer, Heidelberg, 2013.
- [21] W. Subber and A. Sarkar. A domain decomposition method of stochastic PDEs: an iterative solution techniques using a two-level scalable preconditioner. *J. Comput. Phys.*, 257:298–317, 2014.
- [22] A. Toselli and O. Widlund. *Domain decomposition methods—algorithms and theory*, volume 34 of *Springer Series in Computational Mathematics*. Springer-Verlag, Berlin, 2005.
- [23] X. Tu and J. Zhang. Stochastic bddc algorithms. *arXiv preprint arXiv:2510.05993*, 2025.
- [24] E. Ullmann. A Kronecker product preconditioner for stochastic Galerkin finite element discretizations. *SIAM J. Sci. Comput.*, 32(2):923–946, 2010.
- [25] N. Venkovic, P. Mycek, and O. L. Maître. Preconditioners based on voronoi quantizers of random variable coefficients for stochastic elliptic partial differential equations. *arXiv preprint arXiv:2403.07824*, 2024.